Physics – Uspekhi **39** (7) 727 – 743 (1996)

PHYSICS OF OUR DAYS

PACS numbers: 42.50.Ct, 42.50.Dv, **42.52.+x**

One-atom maser and other experiments on cavity quantum electrodynamics

H Walther

Contents

Abstract. The paper gives a brief review of experiments on cavity quantum electrodynamics. Special emphasis is given to recent results on the one-atom maser.

1. Introduction

The simplest and most fundamental system for studying radiation – matter coupling is a single two-level atom interacting with a single mode of an electromagnetic field in a cavity. It received a great deal of attention shortly after the maser was invented, but, at that time, the problem was of purely academic interest since the matrix elements describing the radiation – atom interaction are usually so small that the field of a single photon is not sufficient to lead to an atom field evolution time shorter than the other characteristic times of the system, such as the excited state lifetime, the time of flight of the atom through the cavity and the cavity mode damping time. It was therefore not possible to test experimentally the fundamental theories of radiation – matter interaction, which predict among other effects (see, e.g., Ref. [1]):

(a) a modification of the spontaneous emission rate of a single atom in a resonant cavity,

(b) oscillatory energy exchange between a single atom and the cavity mode, and

(c) the disappearance and quantum revival of Rabi nutation induced in a single atom by a resonant field.

The situation changed abruptly after frequency-tunable lasers became available. They can be used to excite large populations of highly excited atomic states characterised by a high principal quantum number n of the valent electron. These states are generally called Rydberg states, since their energy levels can be described by the simple Rydberg formula. Such excited atoms are very suitable for observing quantum effects in radiation – atom coupling for three reasons. Firstly, the states are very strongly coupled to the radiation field (the induced transition ranges between neighbouring levels scale as n^4); secondly, transitions are in the millimetre wave region so that low-order mode cavities can be made large enough to allow rather long interaction times; finally, Rydberg states have relatively long lifetimes with respect to spontaneous decay [2, 3].

The strong coupling of Rydberg states to radiation resonant with transitions to neighbouring levels can be understood in terms of the correspondence principle: with n increasing the classical evolution frequency of the highly excited electron becomes identical with the frequency of the transition to the neighbouring level. The atom therefore corresponds to a large dipole oscillating with the resonance frequency; the dipole moment is very large since the atomic radius scales as n^2.

In order to understand the modification of the spontaneous emission rate in an external cavity, it is important to remember that in quantum electrodynamics this rate is determined by the density of modes of the electromagnetic field (at the atomic transition frequency ω_0), which is dependent on the square of the frequency. If the atom is not in free space but in a resonant cavity, the continuum of modes is changed into a spectrum of discrete modes and one of them may be in resonance with the atom. The spontaneous decay rate of the atom in the cavity γ_{cav} will then be enhanced in

H Walther Sektion Physik der Universität München and Max-Planck-Institut für Quantenoptik, 85748 Garching, Fed. Rep. of Germany
Tel. (7-095) 135 05 51

Received 2 October 1995
Uspekhi Fizicheskikh Nauk **166** (7) 777 – 794 (1996)
Translated by M L Gorodetskiĭ, edited by L V Semenova, and V B Braginskiĭ as a scientific adviser

relation to that in free space γ_{free} by a factor given by the ratio of the corresponding mode densities:

$$\frac{\gamma_{\text{cav}}}{\gamma_{\text{free}}} = \frac{\rho_{\text{cav}}(\omega_0)}{\rho_{\text{free}}(\omega_0)} = \frac{2\pi Q c^3}{V_{\text{cav}}\omega_0^3} = \frac{Q\lambda_0^3}{4\pi^2 V_{\text{cav}}} ,$$

where V_{cav} is the volume of the cavity and Q is the quality factor of the cavity which expresses the sharpness of the mode. For low-order cavities in the microwave region $V_{\text{cav}} \approx \lambda_0^3$; this means that the spontaneous emission rate is increased by roughly a factor of Q. However, if the cavity is detuned, the decay rate will decrease. In this case, the atom cannot emit a photon, since the cavity is not able to accept it, and therefore the energy has to stay with the atom.

Recently, a number of experiments have been performed with Rydberg atoms to demonstrate this enhancement and inhibition of spontaneous decay in external cavities or cavity-like structures. These experiments will be briefly reviewed in Section 2.

More subtle effects due to the change in the mode density can also be expected: radiation corrections such as the Lamb shift and the anomalous magnetic dipole moment of the electron are modified with respect to the free space value, although the changes are of the same order as the present experimental accuracy. Roughly speaking, one can say that such effects are determined by a change in virtual transitions and not by real transition as in the case of spontaneous decay. A brief review on this topic will be given in Section 3 especially with respect to recent experiments.

Section 4 describes the one-atom maser representing the idealised case of a two-level atom interacting with a single mode of a radiation field. The theory of this system was treated by Jaynes and Cummings [1] many years ago, and we shall concentrate on the dynamics of the atom – field interaction predicted by this theory. A review will be given in Section 5. Some of the features are explicitly a consequence of the quantum nature of the electromagnetic field: the statistical and discrete nature of the photon field leads to new dynamic characteristics such as collapse and revivals in the Rabi nutation. Sections 6 – 11 give an overview on experiments performed with the one-atom maser in connection with the dynamics of the photon exchange between an atom and a cavity mode, the statistics of maser radiation, the observation of quantum jumps, atomic interferometry in the one-atom maser and on planned experiments. In Section 12, the work on optical microlasers will be briefly discussed.

2. Modification of the spontaneous transition rate in confined space

The spontaneous decay rate of an excited atom is proportional to the density of modes of the electromagnetic field above the atomic transition frequency. As a consequence the spontaneous emission rate is increased if the atom is surrounded by a cavity tuned to the transition frequency. This was noted years ago by Purcell [4]; conversely, the decay rate decreases when the cavity is mistuned.

To change the decay rate of an atom, in principle no resonator need to be present; any conducting surface near the radiator affects the mode density and, therefore, the spontaneous radiation rate. Parallel conducting planes can somewhat alter the emission rate but they can only reduce the rate by a factor of 2 owing to the existence of TEM modes, which are independent of the distance between planes.

In order to demonstrate experimentally the modification of the spontaneous decay rate, it is not necessary to go to single-atom densities in both cases. The experiments where spontaneous emission is inhibited can also be performed with large atom numbers. However, in the opposite case, when an increase in the spontaneous rate is observed, a large number of excited atoms may disturb the experiment by induced transitions. The first experimental work on inhibited spontaneous emission was done by Drexhage, Kuhn and Schäfer (for a review see Ref. [5]). The fluorescence of a thin dye film near a mirror was investigated. A reduction of the fluorescence decay by up to 25% results from the standing wave pattern near the mirror. In recent years similar experiments were conducted by de Martini et al. [6]

Inhibited spontaneous emission was also observed by Gabrielse and Dehmelt [7]. In these neat experiments with a single electron stored in a Penning trap they observed that cyclotron orbits show lifetimes which are up to 10 times larger than that calculated for free space. The electrodes of the trap form a cavity which decouple the cyclotron motion from the vacuum radiation field leading to the longer lifetime.

Experiments with Rydberg atoms regarding the inhibition of spontaneous emission have been performed by Hulet et al. [8] and by Jhe et al. [9]. In the latter experiment a 3.4 μm transition was suppressed.

The first observation of enhanced atomic spontaneous emission in a resonant cavity was published by Goy et al. [10]. This experiment was performed with Rydberg atoms of Na excited in the 23rd state in a niobium superconducting cavity resonant at 340 GHz. Cavity tuning-dependent shortening of the lifetime was observed. The cooling of the cavity had the advantage of totally suppressing the blackbody field. The latter effect is completely absent if optical transitions are observed. The first experiments on optical transitions were performed by Feld and collaborators [11]. They succeeded in an enhancement of spontaneous transitions even in higher order optical cavities.

In modern semiconductor devices both electronic and optical properties can be tailored with a high degree of precision. Therefore, electron – hole systems producing recombination radiation analogous to radiating atoms can be localised in cavity-like structures, e.g. in quantum wells. Thus, optical microcavities of half or full wavelength size are obtained. Both suppression and enhancement of spontaneous emission in semiconductor microcavities were demonstrated in experiments by Yamamoto and collaborators [12]. Similar structures have been used by Yablonovitch et al. [13] exhibiting a photonic band gap with spontaneous emission forbidden in certain frequency regions. In recent years it has also become possible to produce microlasers using semiconductor microstructures. These techniques are briefly reviewed in the last section of this paper.

3. Modification of atomic energies in confined space

In Section 2 we have focused on changes of radiation rates of atoms near conducting walls or in cavity-like structures. Next we will discuss the more subtle phenomenon of energy shifts. While radiation rates are modified by the field component in phase quadrature with an atomic dipole, energy shifts are caused by the dispersive part of the interaction or in other words by the field part in phase.

Resonant and nonresonant phenomena have to be distinguished. The resonant self-energy shift of a decaying atomic dipole in the vicinity of a conducting wall can be determined from the average polarisation energy produced by the image dipole field. For distances comparable to the wavelength the near-field condition is satisfied, resulting in the z^{-3} dependence of the static dipole – dipole interaction characteristic for Van der Waals energy; under far-field conditions the distance dependence is given by z^{-1}. The polarisation of the atom by the nonresonant parts of the broad-band electromagnetic field causes energy shifts, of which the Lamb shift is the most prominent one. In the sense of the nonrelativistic treatment by Bethe [14] we can describe the major contribution of that shift as being a result of the emission and reabsorption of virtual photons. It is plausible that just as the real emission of a photon is modified in confined space, so also is the virtual process. The latter 'real' radiation energy shift is thus a consequence of vacuum fluctuations only. It is identical with the energy shift predicted by Casimir and Polder [15] and is analogous to the better-known result of Casimir [16] on the force between two plane neutral conducting plates.

The question of modification of atomic energies in confined space has recently found considerable interest and many calculations of the phenomenon have been performed (for reviews see Refs [17] and [18]). Direct application to the energy shift of Rydberg atoms, which are of special interest for experimental studies, was performed by Barton [19]. In that paper the direct electrostatic interaction with a conducting wall and the radiation induced (retarded) effects were estimated. The result was that in the case of two parallel plates the electrostatic effect is dominant when the distance L between the conducting plates is small, $L < n^3 a_0/\alpha$ (n is the principal quantum number, a_0 is the Bohr radius, and α is the fine-structure constant), and the radiative effect plays a major role when large distances are used, $L > n^3 a_0/\alpha$.

Experiments to measure the Casimir – Polder force using the deflection of atoms between conducting planes were performed in the group of Hinds [20]. They clearly demonstrate the difference of the forces in the near field and far field regime.

In what follows we would like to describe the first experimental data on the radiative shifts of rubidium Rydberg atoms by Wegener at al. [21] and Wegener [22]. For these measurements the Ramsey double-field method is used. The atoms are excited in s-Rydberg states ($n \approx 30$) by two-photon transitions using the light of an ultrastable dye laser, whose line width is less than 10 Hz. The laser intensity was enhanced in a folded cavity which was locked to the laser frequency. Both interaction zones necessary for the Ramsey method were enclosed in this cavity.

Between the two interaction regions the atoms pass through a pair of conducting plates, the distance L between which can be changed. The shift of the Ramsey interferences was measured as a function of the plate distance. Using the Ramsey method has the advantage that the shift can be determined without direct probing of the atoms in the room between the plates.

Especially large level shifts were found when the cut-off frequency of the plate arrangement (mode with polarisation parallel to the planes) agreed with the transition frequency to the next higher or lower Rydberg level [23]. In the present measurements the level shifts are still enhanced by thermal photons. The variation of the shift at the cut-off region amounts to roughly 1 kHz. The line width observed for the Ramsey fringes is 7.4 kHz, corresponding to the time flight between the two laser interaction zones. The pure radiative shift is expected to be observed when the setup is cooled to lower temperatures in order to exclude thermal photons.

We should mention here that the self-energy shift produced by the reflected field of decaying atoms has also been measured [24], this shift is of course much larger than the pure radiative shift of the Casimir – Polder type.

4. Review of the one-atom maser

In the one-atom maser or micromaser a single atom interacts with a single mode of a resonant cavity. This system, at first glance, seems to be another example of a 'Gedanken' experiment, but such a one-atom maser [25] does exist and can in addition be used to study the basic principles of radiation – atom interaction.

The main features of the setup are:

(1) it is the first maser which sustains oscillations with much less than one atom on the average in the cavity;

(2) the maser allows one to study the dynamics of the energy exchange between an atom and a single mode of the cavity field as treated in the Jaynes – Cummings model [1];

(3) the setup makes it possible to study in detail the conditions necessary to obtain nonclassical radiation, especially radiation with sub-Poissonian photon statistics in a maser system directly;

(4) it is possible to study a variety of phenomena of a quantum field such as quantum jumps and nonlocal aspects of the quantum measurement process.

What are the tools that make this device work? It is the enormous progress in superconducting cavities constructing with high quality factors together with the laser preparation of highly excited atoms, i.e. Rydberg atoms, that have made the realisation of such a one-atom maser possible [25]. Rydberg atoms are obtained when one of the outermost electrons of an atom is excited into a level close to the ionisation limit. The main quantum number of the electron is then typically of the order of 60 – 70. Those atoms have quite remarkable properties [2, 3] which make them ideal for the maser experiments: the probability of induced transitions between neighbouring states of a Rydberg atom scales as n^4, where n denotes the principle quantum number. Consequently, a few photons are enough to saturate the transition between adjacent levels. Moreover, the spontaneous lifetime of a highly excited state is very large. We obtain a maser by injecting these Rydberg atoms into a superconducting cavity with a high quality factor. The injection rate is such that on the average there is much less than one atom inside the resonator.

The experimental setup of the one-atom maser is shown in Fig. 1. A highly collimated beam of rubidium atoms passes through a Fizeau velocity selector. Before entering the superconducting cavity, the atoms are excited into the upper maser level $63p_{3/2}$ by the frequency-doubled light of a cw ring dye laser. The superconducting niobium maser cavity is cooled down to a temperature of 0.5 K by means of a ^{3}He cryostat. At this temperature the number of thermal photons in the cavity is about 0.15 at a frequency of 21.5 GHz. The quality factor of the cavity can be as high as 3×10^{10} corresponding to a photon storage time of about 0.2 s. Two maser transitions from the $63p_{3/2}$ level (to $61d_{3/2}$ and to $61d_{5/2}$) are studied. In a new setup equipped with a dilution, refrigerator temperatures

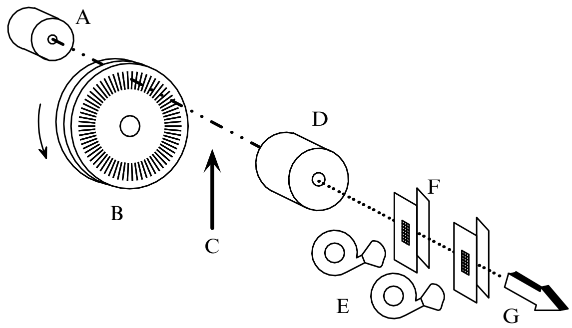

Figure 1. Scheme of the one-atom maser: A — atomic beam oven, B — velocity selector, C — laser excitation, D — maser cavity, E — channeltron detectors, F — field ionisation, G — atomic beam. To suppress blackbody-induced transitions to neighbouring states, the Rydberg atoms are excited inside the liquid-Helium-cooled environment.

in the range of 0.1 K are obtained. Some of the experiments described in this review have been performed with the latter setup.

The Rydberg atoms in the upper and lower maser levels are detected by two separate field ionisation detectors. The field strength is adjusted to ensure that in the first detector the atoms in the upper level are ionised, but not those in the lower level; the lower level atoms are then ionised in the second field.

To demonstrate maser operation, the cavity is tuned over the respective transition and the flux of atoms in the excited state is recorded simultaneously. Figure 2 shows the result for $63p_{3/2} \to 61d_{3/2}$. Transitions from the initially prepared state to the $61d_{3/2}$ level (21.50658 GHz) are detected by a reduction of the electron count rate.

In the case of measurements at a cavity temperature of 0.5 K, shown in Fig. 2, a reduction of the $63p_{3/2}$ signal can be clearly seen for atomic fluxes as small as 1750 atoms s^{-1}. An increase in flux causes power broadening and a small shift. This shift is attributed to the AC Stark effect, caused predominantly by virtual transitions to neighbouring Rydberg levels. Over the range from 1750 to 28000 atoms s^{-1} the field ionisation signal at resonance is independent of the particle flux which indicates that the transition is saturated. This, and the observed power broadening, shows that there is a multiple exchange of photons between Rydberg atoms and the cavity field.

For an average transit time of the Rydberg atoms through the cavity of 50 μs and a flux of 1750 atoms s^{-1} we estimate that approximately 0.09 Rydberg atoms are in the cavity on the average. According to Poisson statistics this implies that more than 90% of the events are due to single atoms. This clearly demonstrates that single atoms are able to maintain a continuous oscillation of the cavity, with a field corresponding to a mean number of photons between unity and several hundred.

Among the studies performed with the one-atom maser are the measurements of the dynamics of the photon exchange between a single atom and a cavity mode [26, 27]. Before we discuss some experiments with the one-atom maser, the theory will be briefly reviewed.

5. Theory of the one-atom maser

The simplest form of interaction between a two-level atom and a single quantised mode of the electromagnetic field is

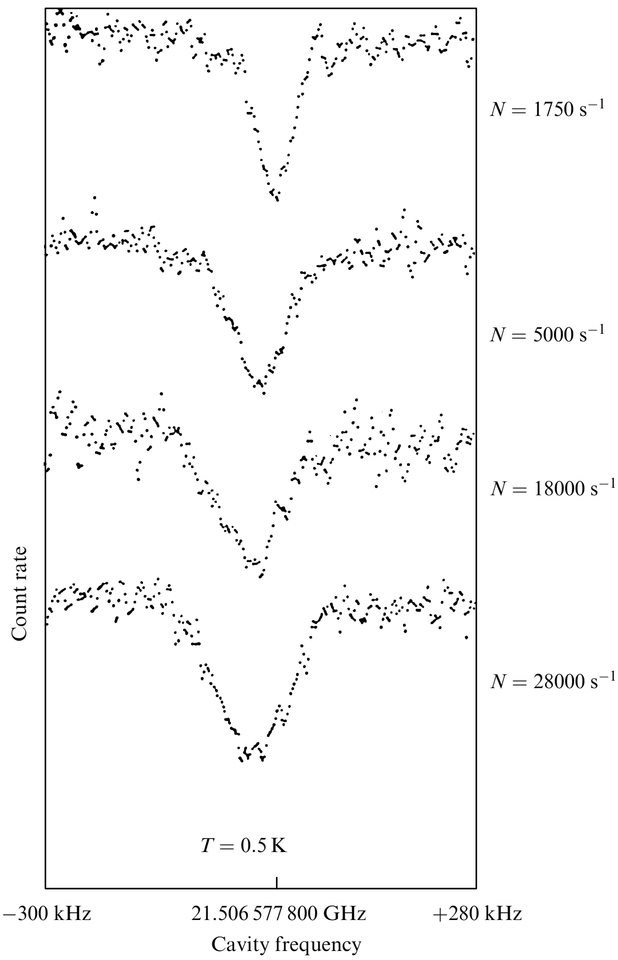

Figure 2. A maser transition $63p_{3/2} \to 61d_{3/2}$ (21.506 577 800 GHz) of the one-atom maser manifests itself in a decrease of ^{85}Rb atoms in the excited state. The flux of excited atoms N governs the pump intensity. Power broadening of the resonance line demonstrates the multiple exchange of a photon between the cavity field and the atom passing through the resonator.

described by the Jaynes – Cummings Hamiltonian [1, 28]

$$H = \frac{1}{2}\,\hbar\omega_0\sigma_z + \hbar\omega a^\dagger a + \hbar(g a^\dagger \sigma_- + \text{adj.}) = H_0 + V\,,$$

where

$$H_0 = \frac{1}{2}\,\hbar\omega_0\sigma_z + \hbar\omega a^\dagger a\,, \qquad V = \hbar(g a^\dagger \sigma_- + \text{adj.})\,.$$

Here, ω_0 is the atomic transition frequency, ω is the field frequency, a and $a^\dagger$ are the photon annihilation and creation operators of the field mode, with $[a, a^\dagger] = 1$, σ_z, σ_+ and σ_- are atomic pseudo-spin operators, while $[\sigma_+, \sigma_-] = \sigma_z$, and

$$g = \frac{pE_\omega}{2\hbar}\,\sin(KZ)$$

is the electric dipole matrix element at the location Z of the atom, where E_ω is the 'electric field per photon', $E_\omega = (\hbar\omega/\varepsilon_0 V)^{1/2}$.

The Jaynes – Cummings model plays a central role in quantum optics owing to several reasons: it gives the simplest description of Rabi flopping in a quantised field and the simplest illustration of spontaneous emission; furthermore, it can be solved exactly and thus describes the true quantum dynamics observed with the one-atom maser such as collapse and revivals of the atomic inversion. The model describes the situation realised in the one-atom maser and allows to investigate in detail the complexities of the atom–field dynamics in the simplest of all situations.

A few results following from the Jaynes–Cummings model are reviewed in light of their relevance to this paper.

The eigenstates of the Jaynes–Cummings Hamiltonian are

$$E_{1n} = \hbar\left[-\frac{1}{2}\,\omega_0 + (n+1)\omega + \frac{1}{2}(\Omega_n + \delta)\right],$$

$$E_{2n} = \hbar\left[\frac{1}{2}\,\omega_0 + n\omega - \frac{1}{2}(\Omega_n + \delta)\right],$$

where $\delta = \omega_0 - \omega$ is the atom–field frequency detuning, Ω_n is the generalised n-photon Rabi-flopping frequency

$$\Omega_n = \sqrt{4g^2(n+1) + \delta^2}\,.$$

The corresponding eigenvalues are those of the dressed atom:

$$|1, n\rangle = \sin\theta_n|a, n\rangle + \cos\theta_n|b, n+1\rangle\,,$$

$$|2, n\rangle = \cos\theta_n|a, n\rangle - \sin\theta_n|b, n+1\rangle\,,$$

where $|a\rangle$ and $|b\rangle$ are the upper and lower atomic states, respectively, and $|n\rangle$ are the number states (i.e. states of well-defined photon number) of the field mode with $a^\dagger a|n\rangle = n|n\rangle$. The angle θ is defined by means of the relations

$$\cos\theta_n = \frac{\Omega_n - \delta}{\left[(\Omega_n - \delta)^2 + 4g^2(n+1)\right]^{1/2}}\,,$$

$$\sin\theta_n = \frac{2g\sqrt{n+1}}{\left[(\Omega_n - \delta)^2 + 4g^2(n+1)\right]^{1/2}}\,.$$

Note, in particular, that

$$\cos 2\theta_n = -\frac{\delta}{\Omega_n}$$

and

$$\sin 2\theta_n = \frac{2g\sqrt{n+1}}{\Omega_n}\,.$$

In the vacuum field at $n = 0$ and on resonance $\omega_0 = \omega$, the dressed states are separated by the frequency $\Omega_0 = 2g$ generally called vacuum Rabi splitting.

One of the interesting phenomena described by the Jaynes–Cummings model is the dynamical behaviour of the system. When we assume that the atom is initially in the upper state $|a\rangle$ and the field is in the number state $|n\rangle$, it follows for the probability of an atom to be in the upper state

$$\left|C_{an}(t)\right|^2 = \cos^2\!\left(gt\sqrt{n+1}\right).$$

This shows that the upper state population oscillates periodically at the Rabi-flopping frequency, similar to the case of classical fields. If the field is initially described by the photon statistics p_n, the above results have to be generalised to:

$$\left|C_a(t)\right|^2 = \sum_n p_n \cos^2\!\left(gt\sqrt{n+1}\right).$$

It has been shown that, in the case where the field mode is initially in a coherent state, $|C_a(t)|^2$ undergoes a collapse followed by a series of revivals [26]. The collapse is due to the destructive interference of quantum Rabi floppings at different frequencies; a similar phenomenon may also occur with a classical field, however, the revivals are a purely quantum mechanical effect that originates in the discreteness of the quantum field. Collapse and revivals have been observed in a micromaser experiment [27]. In this experiment the interaction time of the atoms with the cavity was varied and the probability was investigated that the atoms leave the cavity in the excited state. As will be shown below, the photon statistics in the maser cavity changes when the interaction time is varied, therefore the photon statistics p_n is not a pure distribution. Nevertheless the revival shows up, as was also confirmed in a computer simulation of the results on the basis of the Jaynes–Cummings model [27].

In the following we would like to summarise the results of the quantum theory of the one-atom maser. Since the atom–field interaction takes place in a closed single mode cavity, there is no spontaneous emission rate into free space modes. Owing to the extremely high quality factors achieved in the superconducting cavities, the photon lifetime is extremely long compared to the transit time of the atoms through the resonator. This means that cavity damping can be practically ignored while an atom interacts with the field. Since the atomic flux is kept so small as to have at most one atom inside the cavity at a time, the cavity is therefore empty most of the time and cavity damping can be disregarded during the rare instances when an atom interacts with the cavity mode.

The one-atom maser theory is therefore based on the following strategy [29]: while an atom is in the cavity, the coupled atom–field system is described by the Jaynes–Cummings Hamiltonian and for the interval between atoms the evolution of the field density matrix is described by a master equation considering damping and in addition the mean number of thermal photons in the cavity.

Besides this microscopic theory there is also a macroscopic theory based on the quantum theory of the laser [30]. The resulting probability distribution of the photons depends characteristically on the pump rate and on the interaction time t_{int} of the atoms with the cavity field. One obtains the following result for the probability of finding n photons in the maser cavity $P(n)$ in steady state:

$$P(n) = P_0\left[\frac{n_{\mathrm{b}}}{n_{\mathrm{b}}+1}\right]^n \prod_{m=1}^{n}\left[1 + \frac{N}{n_{\mathrm{b}}\gamma}\,\frac{\sin^2(g\sqrt{m}t_{\mathrm{int}})}{m}\right],$$

with N being the atomic pump rate; n_{b} is the thermal photon number and γ is the cavity decay rate. P_0 is determined by the normalisation condition $\sum P(n) = 1$. One can now evaluate the mean photon number $\langle n\rangle$ and the field variance in the form of the Q_{f} parameter:

$$Q_{\mathrm{f}} = \frac{\langle n^2\rangle - \langle n\rangle^2 - \langle n\rangle}{\langle n\rangle}\,.$$

Figure 3 shows the mean photon number as a function of the interaction time of the atoms with the cavity. The photon number is scaled to $N_{\rm ex}$; here $N_{\rm ex}$ is the average number of atoms that enter the cavity during the cavity decay time $N_{\rm ex} = N/\gamma$. The maser thresholds occurs at $\Theta = 1$ and regions of sub-Poissonian photon statistics are between $\Theta = \pi$ and 2π as well as between 3π and 4π. The sub-Poissonian character leads to a negative $Q_{\rm f}$. A large negative value is obtained close before 2π [28, 29].

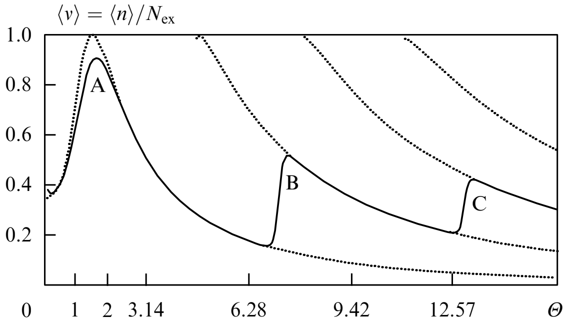

Figure 3. The mean value of the photon number $v = n/N_{\rm ex}$ versus the pump parameter Θ, where the value of Θ is changed via $N_{\rm ex}$. The solid line represents the micromaser solution for $\Omega = 36$ kHz, $t_{\rm int} = 35$ μs, and temperature $T = 0.15$ K. The dotted lines are semiclassical steady state solutions corresponding to fixed stable gain – loss equilibrium photon numbers. The crossing points between a line $\Theta = \text{const}$ and the dotted lines correspond to the values where minima in the Fokker – Planck potential $V(v)$ occur.

To get a more intuitive insight into this effect we recall that the Fizeau velocity selector preselects the velocity of the atoms. Hence, the interaction time is well defined, which leads to conditions usually not achievable in standard masers. This has a very important consequence when the intensity of the maser field grows as more and more atoms transfer their excitation energy to the field: even in the absence of dissipation this increase in photon number is halted when the Rabi frequency increasing leads to a situation where the atoms reabsorb the photon and leave the cavity in the upper state. This situation is close to a quantum non-demolition case. For any photon number this situation can be achieved by appropriate adjusting of the atoms velocity. Then the number distribution of the photons in the cavity is sub-Poissonian.

Unfortunately, the measurement of the nonclassical photon statistics in the cavity is not straightforward. The measurement process of the field involves the coupling to a measuring device, whereby losses lead inevitably to a destruction of the nonclassical properties. The ultimate technique to obtain information about the field employs the Rydberg atoms themselves: for this purpose the population and the statistics of the atoms in the upper and lower maser levels are probed when they leave the cavity. Accordingly, the atoms play a double role: (i) they pump the cavity and (ii) they are used for the diagnostics. These two roles interfere with one another because the detection of the atom in a known final state leads to a quantum mechanical reduction of the photon state inside the resonator. Frequent detection is accompanied by quasipermanent state reduction which can prevent the cavity field from relaxing to the steady state that would be reached if the atoms were left unobserved. Nevertheless, the steady state properties determine the statistics of the clicks recorded by the atom detectors.

The theoretical treatment of the one-atom maser produces predictions about both the photon field and the emerging atoms. Only the latter can be tested experimentally, and the success of such tests feeds our confidence in the predictions about the quantised radiation field inside the cavity. The pump atoms are statistically independent in the standard one-atom-maser experiments, so that their arrival times are subject to a Poissonian statistics; we shall, therefore, restrict the discussion to this standard Poissonian situation.

Inasmuch as the atoms arrive at random, they are recorded at equally random times, and so the only reproducible data are statistical. Consequently, one is led to studying the statistics of the detector clicks. Numerical simulations investigating the effect of repeated atomic measurements on the evolution of the cavity field have been performed by Meystre [31] as well as Meystre and Wright [32]. The relation between the counting statistics of the detected atoms emerging from the resonator and the photon-number statistics of the field inside the cavity has been studied analytically by Rempe and Walther [33] as well as by Paul and Richter [34]. In Ref. [33] the results are also compared with numerical simulations showing good agreement; experimental results are reported by Rempe et al. [35].

In a recent paper a general method for the computation of various statistical properties of the click distribution was presented [36]. This method does not resort to numerical simulations. Naturally, the efficiencies of the detectors (far from the ideal 100%, unfortunately) are taken into account. The central tool used in those calculations is a nonlinear master equation that governs the dynamics of the photon field in the periods between the detector clicks. The nonlinearity arises from the necessity to distinguish between the notions of observation and detection. When the detectors are active, all emerging atoms are observed but only a fraction is actually detected. Most of the time the experimenter observes but does not detect — he listens but does not hear.

In another approach, on the basis of the concept of light beams counting statistics, atomic counting probability, waiting-time distribution, and the 'two-atom correlation' function for a Poissonian atomic beam exciting the micromaser cavity are also calculated. In an analytic treatment it is shown how the waiting-time distribution converges into the atom correlation function for vanishing detection efficiency [37].

Under steady state conditions, as mentioned above, the photon number and the photon statistics of the maser field are essentially determined by the dimensionless parameter Θ (see also Section 8). The quantity $\langle v \rangle = \langle n \rangle / N_{\rm ex}$ shows the following generic behaviour (see Fig. 3): it suddenly increases at the threshold value $\Theta = 1$ and reaches a maximum for $\Theta \approx 2$. As Θ further increases, $\langle v \rangle$ decreases and reaches a minimum at $\Theta \approx 2\pi$, and then abruptly increases to a second maximum. This general type of behaviour recurs roughly at integer multiples of 2π, but becomes less pronounced with an increase in Θ. The reason for the periodic maxima of $\langle v \rangle$ is that for $\Theta \approx 2\pi$ and multiples thereof, the pump atoms perform an almost integer number of full Rabi flopping cycles, and start to flip over at a slightly larger value of Θ, which leads to enhanced photon emission. The maser threshold at $\Theta = 1$ shows the characteristics of a continuous phase transition, whereas the subsequent maxima in $\langle v \rangle$ can be interpreted as first-order phase transitions [28, 29]. In the intervals between the phase-transition points, the photon statistics is mostly sub-Poissonian. The field is super-Poissonian for all phase transitions, the large photon number fluctuations above $\Theta = 2\pi$ and multiples thereof being caused by the presence of two maxima in the photon number distribution $P(n)$. They result from the fact that atoms in the upper maser level may or may not tip over to the lower level.

The phenomenon of the two coexisting neighbouring maxima in $P(n)$ was also studied in a semi-heuristic Fokker – Planck (FP) approach [29]. There, the photon number distribution $P(n)$ is replaced by a probability function $P(\nu, \tau)$ with continuous variables $\tau = t/\tau_{\mathrm{cav}}$ and $\nu(n) = n/N_{\mathrm{ex}}$, the latter replacing the photon number n. The steady state solution, obtained for $P(\nu, \tau), \tau \gg 1$, can be constructed by means of an effective potential $V(\nu)$ showing minima at positions where maxima of $P(\nu, \tau), \tau \gg 1$ are found. Close to $\Theta = 2\pi$ and multiples thereof, the effective potential $V(\nu)$ exhibits two equally attractive minima located at stable gain – loss equilibrium points of maser operation. The mechanism at the phase transitions mentioned is still the same: a minimum of $V(\nu)$ loses its global character when Θ is increased, and is replaced in this role by the next one. This reasoning is a variation of the Landau theory of first-order phase transitions, with $\sqrt{(\nu)}$ being the order parameter. This analogy actually leads to the notion that in the limit $N_{\mathrm{ex}} \to \infty$ the change in the micromaser field around integer multiples of $\Theta = 2\pi$ can be interpreted as first-order phase transitions.

In the region of the first-order phase transitions long field evolution time constants τ_{field} are expected. This phenomenon was experimentally demonstrated, as well as related phenomena, such as spontaneous quantum jumps between equally attractive minima of $V(\nu)$, and bistability and hysteresis [38]. Some of those phenomena are also predicted in the two-photon micromaser [39].

If there are no thermal photons in the cavity (a condition achievable by cooling the resonator to temperatures below 100 mK) very interesting features such as trapping states show up [40]. The investigation of the trapping states is discussed in detail in a recent review [41].

In the following we would like to review several experiments with the one-atom maser. The first one is the observation of the energy exchange of a single atom in a cavity, then the measurement of the photon statistics of the one-atom maser, and the last one is the observation of quantum jumps and bistability in the maser field at the first- order phase transition points. Then we discuss a quite recent experiment on atomic interferometry in the micromaser.

6. Dynamics of a single atom

With very low atomic beam fluxes, the cavity of the single-atom maser contains essentially thermal photons only, whose number varies randomly, obeying the Bose – Einstein statistics. At high fluxes, the atoms deposit energy in the cavity and the maser reaches the threshold so that the number of photons stored in the cavity increases and their statistics changes.

For a coherent field the probability distribution is Poissonian, which results in a dephasing of the Rabi oscillations, and therefore the envelope of $P_{\mathrm{e}}(t)$, the probability of finding the atom in the upper maser level, collapses. After the collapse, $P_{\mathrm{e}}(t)$ starts oscillating again in a very complex way. Such changes recur periodically, the time interval being proportional to the square root of the photon number stored in the cavity. Both collapse and revival in the coherent state are pure quantum features with no classical counterpart (see, e.g., Ref. [26]).

Collapse and revival also occur in the case of a thermal Bose – Einstein field where the spread in the photon number is far larger than for a coherent state, and the collapse time is much shorter. In addition, revivals overlap completely and interfere, producing a very irregular time evolution. On the other hand, a classical thermal field represented by an exponential distribution of the intensity shows collapse but no revival at all. From this it follows that revivals are pure quantum features of the thermal radiation field, whereas the collapse is less clear-cut as a quantum effect [42, 43].

The above-mentioned effects have been demonstrated experimentally by Rempe et al. [27], using the Fizeau velocity selector to vary the interaction time of the atoms with the cavity (see Fig. 1). Figure 4 shows a series of measurements obtained with the single-atom maser, where $P_{\mathrm{e}}(t)$ is plotted against interaction time for different atomic fluxes N. The strong variation of $P_{\mathrm{e}}(t)$ for interaction times between 50 and 80 μs disappears for larger N and a revival shows up for $N = 3000\ \mathrm{s}^{-1}$ for interaction times larger than 140 μs. The average photon number in the cavity varies between 2.5 and 5,

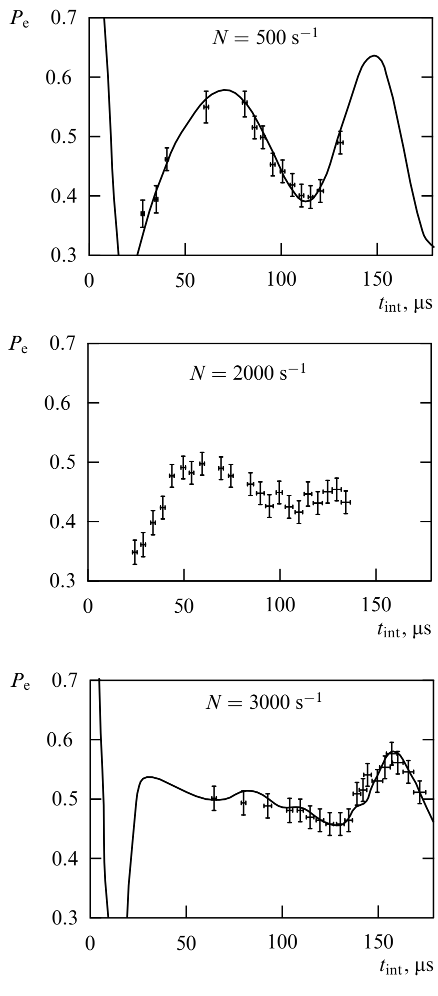

Figure 4. Quantum collapse and revival in the one-atom maser (^{85}Rb $63p_{3/2} \to 61d_{5/2}$). Plotted is the probability $P_{\mathrm{e}}(t_{\mathrm{int}})$ of finding the atom in the upper maser level for different fluxes N of the atomic beam (t_{int} is the time of flight of the atoms through the cavity). The measurements were made with a cavity at 2.5 K [27]. The solid lines correspond to the Jaynes – Cummings model.

about 2 photons being due to the blackbody field corresponding to a temperature of 2.5 K.

7. Sub-Poissonian photon statistics in the micromaser

One of the most interesting questions in connection with the one-atom maser is the photon statistics of the electromagnetic field generated in the superconducting cavity. This problem will be discussed in the following section.

Electromagnetic radiation may exhibit nonclassical properties (for reviews see Refs [44, 45]) that cannot be explained by classical theory. We know of essentially three phenomena which demonstrate the nonclassical character of light: photon antibunching [46, 47], sub-Poissonian photon statistics [48, 49] and squeezing (see, e.g., Ref. [50]). Methods of nonlinear optics are most often employed to generate nonclassical radiation. However, the fluorescence light from a single atom caught in a trap also displays nonclassical features [49, 51].

Another nonclassical light generator is the one-atom maser. The Fizeau velocity selector, it will be recalled, preselects the velocity of the atoms; hence the interaction time is well-defined, leading to conditions usually not achievable in standard masers. This has a very important consequence when the intensity of the maser field grows as more and more atoms give their excitation energy to the field: even in the absence of dissipation, this increase in photon number is stopped when the increasing Rabi frequency leads to a situation where the atoms reabsorb the photon and leave the cavity in the upper state. For any photon number this can be achieved by appropriate adjusting of the atoms velocity. In this case the maser field is not changed any more and the number distribution of the photons in the cavity is sub-Poissonian [29, 30], i.e. narrower than a Poisson distribution. Even a number state, i.e. a state of well-defined photon number, can be generated as shown in Ref. [52] by using a cavity with a high enough quality factor. If there are no thermal photons in the cavity (a condition achievable by cooling the resonator to an extremely low temperature) very interesting features such as trapping states show up [40]. In addition, steady state macroscopic quantum superpositions can be generated in the one-atom maser field when two-level atoms are injected in a coherent superposition of their upper and lower states [50].

The measurement of the photon statistics via the dynamic behaviour of the atoms in the radiation field, i.e. via collapse and revival of the Rabi oscillations, is one possibility to obtain information about the field. However, since the photon statistics depends on the interaction time, which has to be changed when collapse and revivals are measured, it is much better to probe the population of the atoms in the upper and lower maser levels when they leave the cavity. In this case, the interaction time is kept constant. Moreover, this measurement is relatively easy since electric fields can be used to perform selective ionisation of the atoms. The detection sensitivity is sufficient for the atomic statistics to be investigated. This technique maps the photon statistics of the field inside the cavity via the atomic statistics, and then the number of maser photons can be inferred from the number of atoms detected in the lower level. In addition, the variance of the photon number distribution can be deduced from the number fluctuations of the lower-level atoms [33]. In the experiment we are therefore mainly interested in the atoms in the lower maser level. Experiments carried out along these lines are described in the next section [35].

8. Experimental results. A sub-Poissonian beam of atoms

Under steady state conditions, the photon statistics of the field is essentially determined by the dimensionless parameter $\Theta = (N_{\rm ex} + 1)^{1/2}\Omega t_{\rm int}$, which can be understood as a pump parameter for the one-atom maser [29]. Here, $N_{\rm ex}$ is the average number of atoms that enter the cavity during the lifetime of the field, $t_{\rm int}$ is the time of flight of the atoms through the cavity, and Ω is the atom – field coupling constant (one-photon Rabi frequency). The one-atom maser threshold is reached for $\Theta = 1$. At this value and also at $\Theta = 2\pi$ and integer multiples thereof, the photon statistics is super-Poissonian. At these points the maser field undergoes first-order phase transitions [29]. In the regions between those points sub-Poissonian statistics are expected. The experimental investigation of the photon number fluctuation is the subject of the following discussion.

In the experiments [35] the number N of atoms in the lower maser level is counted for a fixed time interval T roughly equal to the storage time $T_{\rm cav}$ of the cavity. By repeating this measurement many times the probability distribution $P(N)$ of finding N atoms in the lower level is obtained. The normalised variance

$$Q_{\rm a} = \frac{\langle N^2 \rangle - \langle N \rangle^2 - \langle N \rangle}{\langle N \rangle}$$

is evaluated and is used to characterise the deviation from Poissonian statistics. A negative (positive) $Q_{\rm a}$ value indicates sub-Poissonian (super-Poissonian) statistics, while $Q_{\rm a} = 0$ corresponds to a Poisson distribution with $\langle N^2 \rangle - \langle N \rangle^2 = \langle N \rangle$. The atomic $Q_{\rm a}$ is related to the normalised variance $Q_{\rm f}$ of the photon number by the formula [33]

$$Q_{\rm a} = \epsilon P_{\rm g} Q_{\rm f}(2 + Q_{\rm f}) \,, \qquad (1)$$

with $P_{\rm g}$ denoting the probability of finding an atom in the lower maser level. It follows from Eqn (1) that the nonclassical photon statistics can be observed via sub-Poissonian atomic statistics. The detection efficiency ϵ for the Rydberg atoms reduces the sub-Poissonian character of the experimental result. The detection efficiency was 10% in experiment [35]; this includes the natural decay of the Rydberg states between the cavity and the field ionisation detection [35].

We start the discussion of the experimental results by describing measurements in the build-up period of the maser field. For this purpose, the mean number of atoms passing through the cavity during a fixed sampling time interval shorter than the cavity decay time is varied. For each flux, the normalised variance $Q_{\rm a}$ of the probability distribution of atoms detected in both the upper and the lower maser levels is determined. Experimental results are plotted in Fig. 5. Open circles (full circles) represent the normalised variance of atoms in the lower (upper) maser level leading to a sub-Poissonian (super-Poissonian) atom statistics. About 20,000 experiments are averaged for each data point to keep the uncertainty of $Q_{\rm a}$ below 1%. For a low temperature of the atomic beam oven, the horizontal error bars are determined by the Poisson statistics of the total flux of atoms. This statistics is measured with the cavity out of resonance so that all atoms leave the cavity in the upper level. The result is given by a Poisson distribution with $Q_a = 0$.

The two solid lines are calculated by a numerical simulation of the maser process which explicitly takes into account the measurement of atoms and the corresponding change of the cavity photon statistics. Details of this procedure are given in Ref. [33]. For a comparison with the results of Fig. 5 the method was extended to the transient regime of an increasing maser field starting from the thermal field of 0.5 K. The detection efficiency of atoms in the lower and upper maser levels amounts to 10% and 7%, respectively. In the simulation, the Poisson statistics of the flux, the temperature of the cavity field (0.5 K), and the damping of the maser field in the time interval between adjacent atoms are also considered. The agreement between the numerical simulation and the experimental results is good.

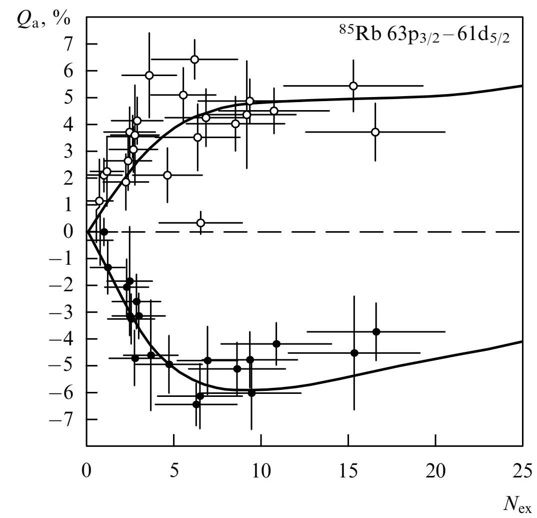

Figure 5. Variance Q_a of the atoms in the lower (○) and upper (●) levels as a function of the total number of atoms crossing the cavity.

The sub-Poissonian statistics of atoms in the lower level proves the nonclassical character of the maser field. As is expected from simple statistical arguments, the probability distribution of atoms in the upper maser level is always super-Poissonian. With the single-photon Rabi frequency given by $g = 44$ kHz, two photons ($n = 2$) are able to induce a 2π Rabi nutation of the atom during the atom–field interaction time of $t_{int} = 40$ μs:

$$2g(n+1)^{1/2} t_{int} = 6.10\,.$$

This number is slightly smaller than 2π to reduce the influence of the velocity distribution on the maser photon statistics. The simulation shows that, averaged over many experiments, the probability distribution of finding n maser photons after about 8 atoms have crossed the cavity has a mean of $\langle n \rangle = 2$ and a variance of $\langle n^2 \rangle - \langle n \rangle^2 = 0.2\langle n \rangle$. In the experiment, this value corresponds to $Q_a = -6 \times 10^{-2}$. Figure 5 shows that for a higher flux of atoms (more than 20), the normalised variance of the probability distribution for atoms in the lower level increases slowly, indicating that the 2π trapping condition is not exactly fulfilled.

We shall now continue the discussion of our results on the maser in steady state. Experimental results for the transition $63p_{3/2} \to 61d_{3/2}$ are shown in Fig. 6. The measured normalised variance Q_a is plotted as a function of the flux of atoms. The atom–field interaction time is fixed at $t_{int} = 50$ μs. The atom–field coupling constant g is rather small for this transition, $g = 10$ kHz. A relatively high flux of atoms $N_{ex} > 10$ is therefore needed to drive the one-atom maser above threshold. The large positive Q_a observed in the experiment proves the large intensity fluctuations at the onset of maser oscillation at $\Theta = 1$. The solid line is plotted according to Eqn (1) using the theoretical predictions for Q_f of the photon statistics [29, 30]. The error in the signal follows from the statistics of the counting distribution $P(N)$. About 2×10^4 measurement intervals are needed to keep the error of Q_a below 1%. The statistics of the atomic beam is measured with a detuned cavity. The result is a Poisson distribution. The error bars of the flux follow from this measurement. The agreement between theory and experiment is good.

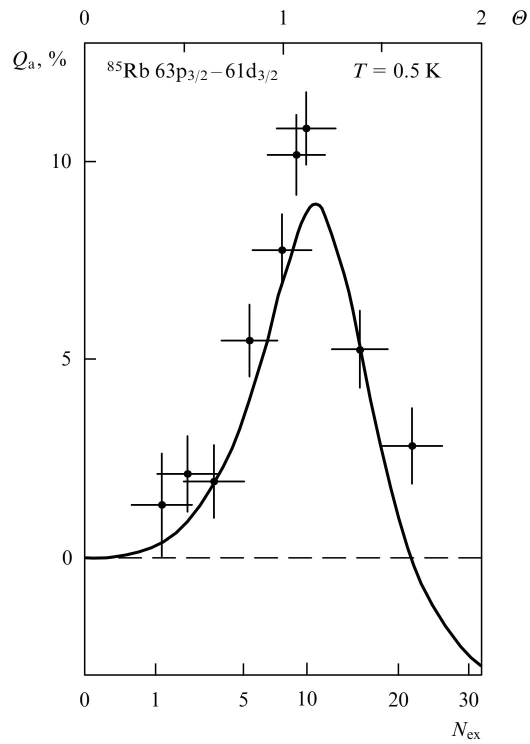

Figure 6. Variance Q_a of the atoms in the lower maser level as a function of flux N_{ex} near the onset of maser oscillation for $63p_{3/2} \to 61d_{3/2}$ [35].

The nonclassical photon statistics of the one-atom maser is observed at a higher flux of atoms or at a larger atom–field coupling constant. Therefore the $63p_{3/2} \to 61d_{5/2}$ maser transition with $g = 44$ kHz was also studied. Experimental results for this transition are shown in Fig. 7. Fast atoms with an atom–cavity interaction time of $t_{int} = 35$ μs are used. A very low flux of atoms of $N_{ex} > 1$ is already sufficient to generate a nonclassical maser field. This is the case since the vacuum field initiates a transition of the atom to the lower maser level, thus driving the maser above threshold. The sub-Poissonian statistics can be understood from Fig. 8, where the probability of finding the atom in the upper level is plotted as a function of the atomic flux. The oscillation observed is closely related to the Rabi nutation induced by the maser field. The solid curve was calculated according to the one-atom maser theory with a velocity dispersion of 4%. A higher

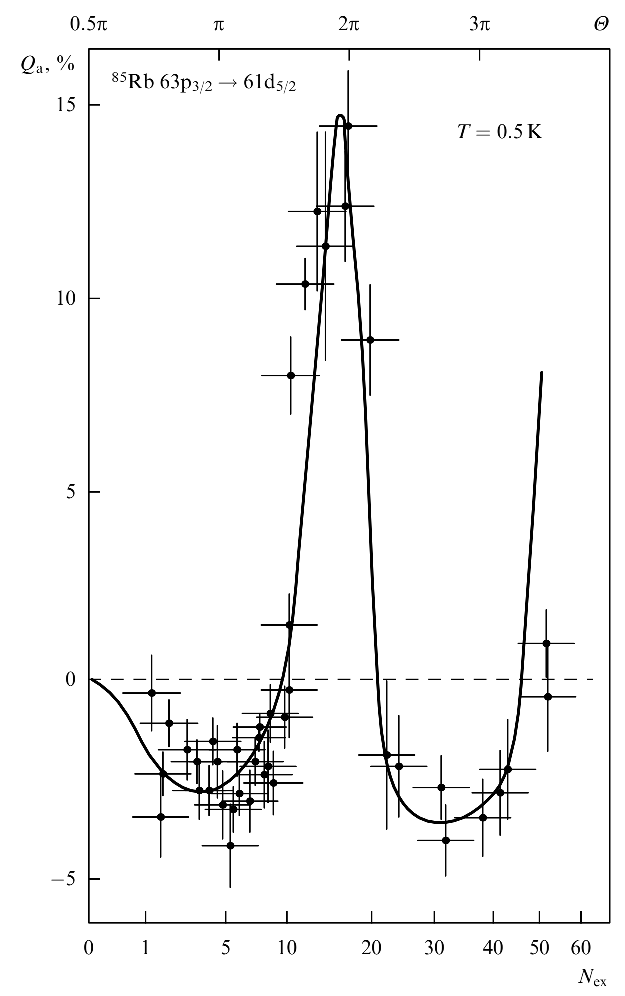

Figure 7. Variance Q_a of the atoms in the lower maser level as a function of flux N_{ex} near the onset of maser oscillation for $63p_{3/2} \to 61d_{5/2}$ [35].

flux generally leads to a higher photon number, but for $N_{ex} < 10$ the probability of finding the atom in the lower level decreases. An increase in the photon number is therefore counterbalanced by the fact that the probability of photon emission in the cavity is reduced. This negative feedback leads to a stabilisation of the photon number [33]. The feedback changes sign at a flux $N_{ex} \approx 10$, where the second maser phase transition is observed at $\Theta = 2\pi$. This is again characterised by large fluctuations of the photon number. Here the probability of finding an atom in the lower level increases with increasing flux. For even higher fluxes, the state of the field is again highly nonclassical. The solid line in Fig. 7 represents the results of the one-atom maser theory using Eqn (1) to calculate Q_a. Agreement with the experiment is very good.

The sub-Poissonian statistics of atoms near $N_{ex} = 30$, $Q_a = -4\%$, and $P_e = 0.45$ (see Fig. 7) is generated by a photon field with a variance $\langle n^2 \rangle - \langle n \rangle^2 = 0.3\langle n \rangle$, which is 70% below the shot noise level. Again, this result agrees with the prediction of the theory. The mean number of photons in the cavity is about 2 and 13 in the regions $N_{ex} \approx 3$ and $N_{ex} \approx 30$, respectively. Near $N_{ex} \approx 15$, the photon number abruptly changes between these two values. The next maser phase transition with a super-Poissonian photon number distribution occurs above $N_{ex} \approx 50$.

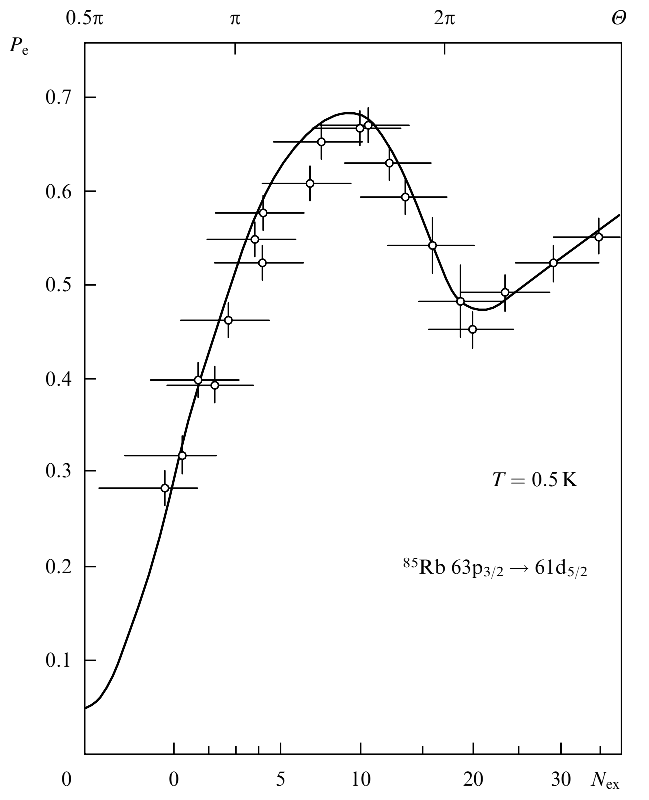

Figure 8. Probability P_e of finding the atom in the upper maser level ($63p_{3/2} \to 61d_{5/2}$) as a function of the atomic flux N_{ex}.

The sub-Poissonian statistics is closely related to the phenomenon of antibunching, for which the probability of detecting a next event shows a minimum immediately after a triggering event. The duration of the time interval with reduced probability is of the order of the coherence time of the radiation field. In our case this time is determined by the storage time of the photons. The Q_a value therefore depends on the measuring interval T. Experimental results for a flux $N_{ex} \approx 30$ are shown in Fig. 9. The measured Q_a value approaches a time-independent value for $T > T_{cav}$. For very short sampling intervals, the statistics of atoms in the lower

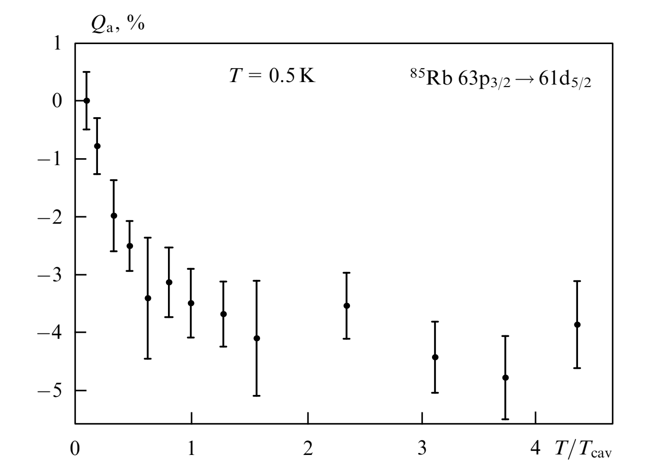

Figure 9. Variance Q_a of the atoms in the lower maser level as a function of the measurement time interval T for a flux $N_{ex} \approx 30$ [35].

level shows a Poisson distribution. This means that the cavity cannot stabilise the flux of atoms in the lower level on a time scale which is short in relation to the intrinsic cavity damping time.

We want to emphasise that the reason for the sub-Poissonian atomic statistics is the following: a changing flux of atoms changes the Rabi frequency via the stored photon number in the cavity. By the interaction time adjusting , the phase of the Rabi-nutation cycle can be chosen so that the probability for the atoms leaving the cavity in the upper maser level increases when the flux and therefore the photon number is enlarged or vice versa. We observe sub-Poissonian atomic statistics in the case where the number of atoms in the lower state decreases with an increase in the flux and the number of photons in the cavity. The same argument can be applied to understand the nonclassical photon number in the cavity: any deviation of the number of light quanta from its mean value is counterbalanced by a correspondingly changed probability of photon emission for the atoms. This effect leads to a natural stabilisation of the maser intensity by a feedback loop incorporated into the dynamics of the coupled atom – field system. This feedback mechanism is also demonstrated when the anticorrelation of the coupled atoms leaving the cavity in the lower state is investigated. Measurements of these ‘antibunching’ phenomena for atoms are described as follows.

For steady state conditions, experimental results are displayed in Fig. 10. Plotted is the probability $g^{(2)}(t)$ of finding an atom in the lower maser level $61d_{5/2}$ at time t after a first atom has been detected at $t = 0$. The probability $g^{(2)}(t)$ was calculated from the actual count rate by normalising with the average number of atoms determined in a large time interval. Time is given in units of photon storage time. The error bar of each data point is determined by the number of about 7000 lower level atoms counted. This corresponds to 2×10^6 atoms that have crossed the cavity during the total measurement time. The detection efficiency is near $\eta = 10\%$. The measurements were taken for $N_{ex} = 30$. The time of flight of the atoms through the cavity was $t_{int} = 37$ μs, leading to $\Theta = 9$.

The fact that anticorrelation is observed shows that the atoms in the lower state are more equally spaced than expected for Poissonian distribution. This means that when two atoms enter the cavity close to each other the second atom performs a transition to the lower state with a reduced probability.

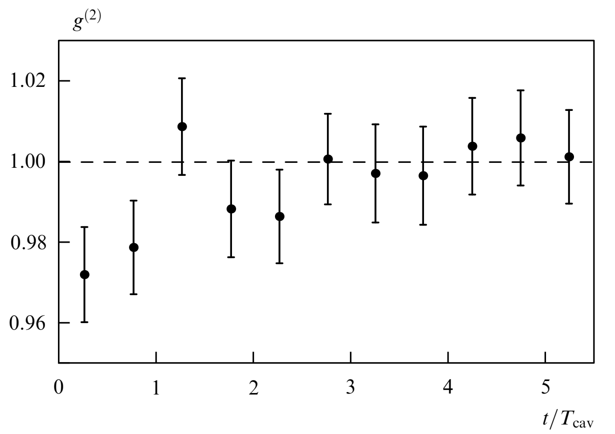

Figure 10. Anticorrelation of atoms in the lower maser state.

The experimental results presented here clearly show the sub-Poissonian photon statistics of a one-atom maser field. An increase in the flux of atoms leads to the predicted second maser phase transition. In addition, the maser experiment leads to an atomic beam with atoms in the lower maser level showing number fluctuations which are up to 40% below those of the Poissonian distribution usually found in atomic beams. This is interesting because atoms in the lower level have emitted a photon to compensate for cavity losses inevitably present under steady state conditions. This is a purely dissipative phenomenon giving rise to fluctuations, nevertheless the atoms still obey sub-Poissonian statistics.

At the end of this section we would like to give a simple physical picture for the reason that sub-Poissonian statistics is observed in the micromaser. The regions where this is the case are slightly below the $\Theta \approx 2\pi$ or multiples thereof. There the atoms enter and leave the cavity in the upper state. That means a measurement of the field is performed without changing the field. This is a situation close to a quantum non-demolition measurement [53]. The measurement process does not introduce additional fluctuations, therefore sub-Poissonian statistics is observed.

9. Quantum jumps of the micromaser field

The setup used for these measurements is similar to that described above. As before, ^{85}Rb atoms were used to pump the maser. They are excited from the $5S_{1/2}, F = 3$ ground state to $63P_{3/2}$, $m_j = \pm 1/2$ states by linearly polarised light of a frequency-doubled cw ring dye laser. The polarisation of the laser light is linear and parallel to the likewise linearly polarised maser field, and therefore only $\Delta m_j = 0$ transitions are excited. Superconducting niobium cavities resonant with the transition to the $61D_{3/2}, m_j = \pm 1/2$ states were used. The experiments were performed in a ^{3}He/^{4}He dilution refrigerator with cavity temperatures $T \approx 0.15$ K. The cavity Q-values ranged from 4×10^9 to 8×10^9. The velocity of the Rydberg atoms and thus the time t_{int} of their interaction with the cavity field were preselected by exciting a particular velocity subgroup with the laser. For this purpose, the laser beam irradiated the atomic beam at an angle of approximately 82°. As a consequence, the UV laser light (linewidth ≈ 2 MHz) is blue-shifted by 50 – 200 MHz by the Doppler effect, depending on the velocity of the atoms [38].

As before, information on the maser field and interaction of the atoms in the cavity can be obtained solely by state-selective field ionisation of the atoms in the upper or lower maser level after they have passed through the cavity. The field ionisation detector was recently modified, so that there is now a detection efficiency of $\eta = (35 \pm 5)\%$. For different t_{int} the atomic inversion has been measured as a function of the pump rate; the coupling constant is about $g = 40$ rad s^{-1}.

Depending on the parameter range, essentially three regimes of the field evolution time constant τ_{field} can be distinguished [38]. We shall restrict our discussion here only to the results for intermediate time constants. The maser operated under steady state conditions close to the second first-order phase transition (C in Fig. 3). The interaction time was $t_{int} = 47$ μs and the cavity decay time was $\tau_{cav} = 60$ ms. The value of N_{ex} necessary to reach the second first-order phase transition was $N_{ex} \approx 200$. For these parameters the two maxima in $P(n)$ are manifested in spontaneous jumps of the maser field between the two maxima with a time constant of approximately 5 s. This fact and the relatively large pump rate lead to the clearly observable field jumps shown in Fig. 11. Due to the large cavity field decay time, the average number of atoms in the cavity was still as low as 0.17. The two discrete values for the counting rates correspond to the metastable operating points of the maser, which correspond to approximately 70 and 140 photons. In the FP description, the two values correspond to two equally attractive minima in the FP potential $V(v)$. If one considers, for instance, the counting rate of lower-state atoms (Fig. 11b), the lower (higher) plateaus correspond to time intervals in the low (high) field metastable operating point. If the actual photon number distribution is averaged over a time interval containing many spontaneous field jumps, the steady state result $P(n)$ of the micromaser theory is recovered.

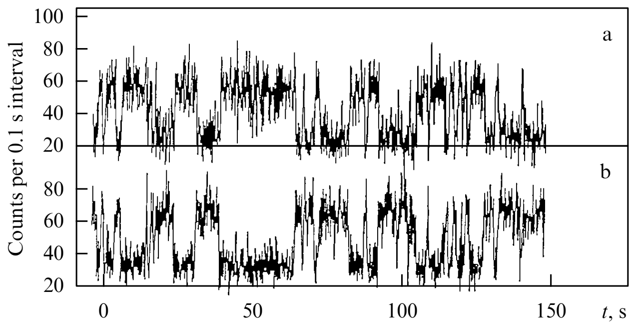

Figure 11. Quantum jumps between two equally stable operation points of the maser field. The channeltron counts are plotted versus time: (a) upper state, (b) lower state.

In a parameter range where switching occurs much faster than in the case shown in Fig. 11, the individual jumps cannot be resolved any more owing to the reduced N_{ex} necessary in this case. Therefore, a different procedure has to be chosen for the investigation. Those experiments will not be discussed here, details are described in Ref. [38].

10. Atomic interferometry in the micromaser

In this section we report on the observation of the maser resonance under conditions where atomic interference phenomena in the cavity become observable. Since a nonclassical field is generated in the maser cavity, we are able to investigate for the first time atomic interference phenomena under the influence of nonclassical radiation; owing to the bistable behaviour of the maser field the interferences show quantum jumps; thus the quantum nature of the field becomes directly observable through the interferences. Interferences occur since a coherent superposition of dressed states is produced by mixing the states at the entrance and exit holes of the cavity. Inside the cavity the dressed states develop differently in time, giving rise to interferences [54] when the maser cavity is tuned through resonance.

The setup used in the experiment is identical to the one described before (see Section 9). However, the flux of atoms through the cavity is by a factor of 5 – 10 higher than that in the previous experiments, where we also used the $63p_{3/2} \rightarrow 61d_{5/2}$ transition. The atoms are excited into the upper maser level, $63p_{3/2}$, when they enter a cylindrical cavity. The velocity of the atoms can be selected by exciting a velocity subgroup. Behind the cavity the atoms are detected in separate detectors for upper and lower maser levels. The Q-value of the cavity was 6×10^9 corresponding to a photon decay time of 42 ms.

Figure 12a shows the standard maser resonance which is obtained when the resonator frequency is tuned. At large values of N_{ex} ($N_{ex} > 89$) sharp, periodic structures appear. These structures consist typically of a smooth red wing and a vertical step on the blue side. The clarity of the pattern rapidly decreases when N_{ex} increases to 190 or beyond. We shall see later that these structures have to be interpreted as interferences. It can be seen that the atom – field resonance frequency is red-shifted with an increase in N_{ex} and reaches 200 kHz for $N_{ex} = 190$. Under these conditions there are roughly 100 photons on the average in the cavity. The large red shift cannot be explained by AC Stark effect, which for 100 photons would amount to about 1 kHz for the transition used. Therefore it is obvious that other reasons must be responsible for the observed shift.

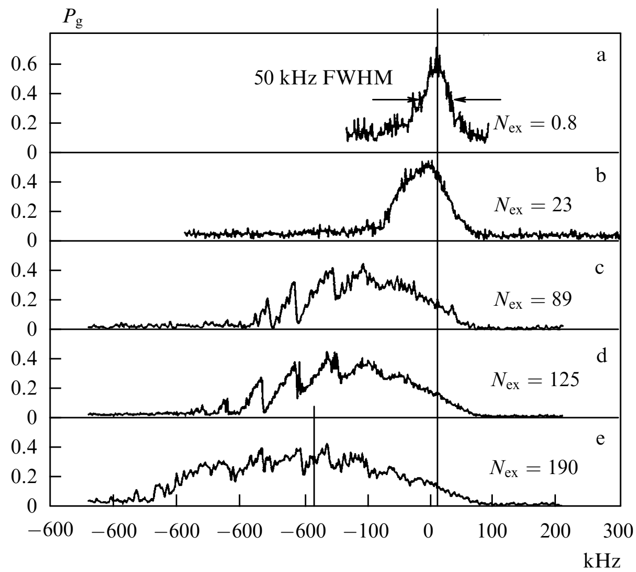

Figure 12. Shift of the maser resonance $63p_{3/2} \rightarrow 61d_{5/2}$ (frequency is 21.456 GHz) for fast atoms ($t_{int} = 35$ μs). (a) The maser line for low pump rate ($N_{ex} < 1$). The FWHM linewidth (50 kHz) sets an upper limit of about 5 mV cm^{-1} to residual stray electric fields in the centre of the cavity. (b) – (e) The resonance lines are taken for the indicated large values of N_{ex}. The plots show that the centre of the maser line shifts by about 2 kHz per photon. In addition, there is considerable field-induced line broadening which is approximately proportional to $\sqrt{N_{ex}}$. For $N_{ex} \geqslant 89$ the lines display periodic structures, which are discussed in the text.

There are small static electric fields in the entrance and exit holes of the cavity. It is supposed that these fields are generated by patch effects at the surface of the niobium metal caused by rubidium atoms from the beam or by microcrystallites formed when the cavities are tempered after machining. The tempering process is necessary to achieve high quality factors. The influence of those stray fields is only observable in the cavity holes; in the centre of the cavity they are negligible owing to the large atom – wall distances.

Figure 13 shows the variation of the structure when the interaction time t_{int} between the atoms and the cavity field is changed. The recording shown in Fig. 13a is the same as in Fig. 12d. For large t_{int} no clear substructures can be observed. In Fig. 13b a substructure is still present on the left side, but it is less pronounced than in Fig 13a. The plots in Fig. 13a,b

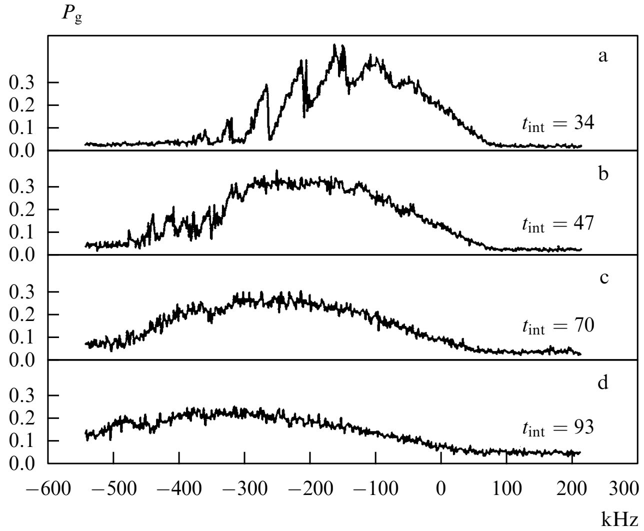

Figure 13. Maser resonance lines for large N_{ex} ($62p_{3/2} \rightarrow 61d_{5/2}$, frequency is 21.456 GHz) and the indicated values of t_{int}. The period and clarity of the additional structures reduce when t_{int} is increased. Furthermore the centre of the resonance shifts to lower frequency with increasing t_{int}.

show that the period of the substructures reduces with an increase in the interaction time. The substructure disappears for $t_{int} > 47$ μs. Furthermore, an increasing shift of the whole structure to low frequencies is observed when t_{int} is increased.

In order to understand the observed structures we have to analyze first the Jaynes–Cummings dynamics of the atoms in the cavity. This treatment is more involved than that in connection with previous experiments, since the higher maser field requires detailed consideration of the field in the periphery of the cavity, where the additional influence of stray electric fields is more important. In subsequent analysis we follow the micromaser theory [29, 30].

The usual formalism for the description of the coupling of an atom to the radiation field is the dressed atom approach [55], which leads to a splitting of the coupled atom–field states, depending on the vacuum Rabi-flopping frequency Ω, the photon number n, and the detuning δ. We face a special situation at the entrance and exit holes of the cavity. There we have a position-dependent variation of the cavity field, as a consequence of which Ω is position dependent. Additional variation results from the stray electric fields in the entrance and exit holes. Owing to the Stark effect these fields lead to a position-dependent atom–field detuning δ.

The Jaynes–Cummings Hamiltonian couples only pairs of dressed states. Therefore, it is sufficient to consider the dynamics within such a pair. In our case the system is in one of the two dressed states prior to the atom–field interaction. For parameters corresponding to the periodic substructures in Figs 12 and 13 the dressed states are mixed only at the beginning and at the end of the atom–field interaction. The mixing at the beginning creates a coherent superposition of the dressed states. Afterwards the system develops adiabatically, whereby the two dressed states accumulate a differential dynamic phase Φ which strongly depends on the cavity frequency. The mixing of the dressed states at the entrance and exit holes of the cavity, in combination with the intermediate adiabatic evolution, generates a situation similar to a Ramsey two-field interaction.

The maximum differential dynamic phase Φ resulting from the maser field alone is roughly 4π under the experimental conditions used here. This is not sufficient to explain the interference pattern of Fig. 12, where we have at least six maxima corresponding to a differential phase of 12π. This means that an additional energy shift differently affecting the upper and lower maser states is present. Such a phenomenon can be caused by the above-mentioned small static electric fields present in the holes of the cavity. The static field causes a position-dependent detuning δ of the atomic transition from the cavity resonance; as a consequence we get an additional differential dynamic phase Φ. In order to interpret the periodic substructures as a result of the variation of Φ with the cavity frequency, the phase Φ has to be calculated from the atomic dynamics in the maser field.

The quantitative calculation can be performed in the following way. First, the variation of the static electric field in the cavity has to be estimated. This is done by numerically solving the Laplace equation with the boundaries of the cavity and assuming a particular field strength in the cavity holes. Then, for different interaction times, photon numbers, and cavity frequencies the dynamics of the atom–field wavefunction is calculated by numerical integration of the Jaynes–Cummings model. This integration has to include the local variation of Ω inside the cavity owing to the mode structure of the microwave field (the TE_{121} mode in our case). Furthermore, the variation of the detuning δ resulting from the static electric fields in the cavity holes has to be considered. In order to use the micromaser model we extract the β_n values, which denote the probabilities of an atom emitting a photon in a field of $n-1$ photons prior to the interaction.

In the second step of the calculation, using the β_n values, the photon number distribution $P(n)$ of the cavity field under steady state conditions is obtained from the recursion formula

$$P(n) = \frac{n_b}{n_b+1}\left(1 + \frac{N_{ex}\langle\beta_n\rangle}{n_b}\right)P(n-1)\,.$$

Here n_b stands for the number of thermal photons. The $\langle\ \rangle$ indicates that the β_n have to be averaged over all statistical fluctuations such as the spread of t_{int} caused by the velocity distribution. With $P(n)$, the average photon number $\langle n\rangle$ and $\langle n\rangle/N_{ex}$ are calculated. The latter quantity corresponds to the probability of finding an atom in the lower state, as do the experimental results displayed in Figs 12 and 13.

A theoretical result of $\langle n\rangle/N_{ex}$ obtained in this way is shown in Fig. 14. Plot *1* shows the maser resonance line expected without any static electric field. By increasing DC field strength in the cavity holes the structure changes with the curve *4* for 309 mV cm^{-1} coming very close to the plots displayed in Figs 12 c, d for $N_{ex} = 89$ and 125 and in Fig. 13a. It should be emphasised that the field values indicated in Fig. 14 correspond to the maximum field strength in the cavity holes. The field value in the central part of the cavity is roughly 100 times smaller and therefore negligent in low-flux maser experiments. Figure 14 also shows that the qualitative structure of the maser line is the same for all fields larger than about 200 mV cm^{-1}. Thus, the conditions required to find the periodic substructures experimentally are not very stringent.

The calculations also reproduce the experimental finding that the maser line shifts to lower frequencies when N_{ex} is

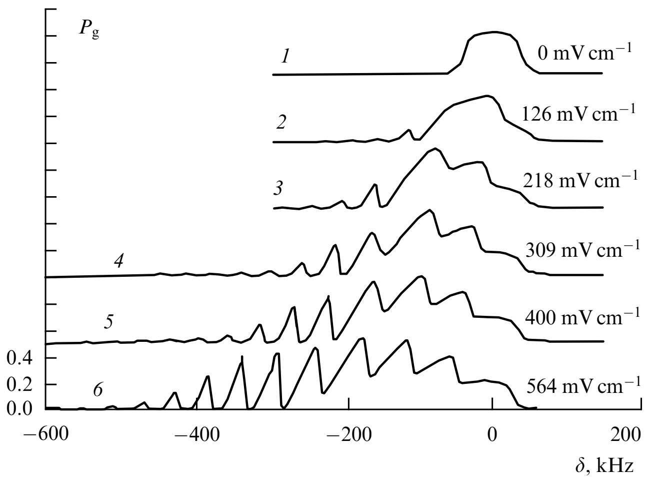

Figure 14. Theoretical maser lines for the indicated values of the static electric field strength in the cavity holes. The theoretical model is explained in the text. In the calculation we use $N_{ex} = 100$ and $\Omega = 45$ krad s^{-1}. The interaction time is $t_{int} = 35$ μs and the RMS deviation of the interaction time is 1 μs. In order to account for the fluctuations of the dynamic phases induced by the inhomogeneity of the stray electric fields, a Gaussian distribution of the atom – field detuning with a RMS deviation of 5 kHz is assumed (see also Ref. [38]).

increased. The mechanism for that can be explained as follows: the blue edge of the maser line does not shift with N_{ex} at all, since this part of the resonance is produced in the central region of the cavity, where practically no static electric fields are present. The low-frequency cutoff of the structure is determined by the location where the mixing of the dressed states occurs. With a decrease in cavity frequency those points shift closer to the entrance and exit holes, with the difference between the particular cavity frequency and the unperturbed atomic resonance frequency giving a measure of the static electric field at the mixing locations. Closer to the holes the passage behaviour of the atoms through the mixing locations becomes non-adiabatic for the following reasons. Firstly, the maser field strength decreases towards the holes. This leads to a reduced repulsion of the dressed states. Secondly, the stray electric field strongly increases towards the holes. This implies a larger differential slope of the dressed state energies at the mixing locations, and therefore leads to a stronger non-adiabatic passage. At the same time the observed signal extends further to the 'red' spectral region. Since the photon emission probabilities β_n decrease towards longer wavelength their behaviour finally defines the red boundary of the maser resonance line. As N_{ex} increases the photon number n rises. As for larger n values the photon emission probabilities β_n get larger, also an increase in N_{ex} leads to an extension of the range of the signal to lower frequencies. This theoretical expectation is in agreement with the experimental observation.

In the experiment it is also found that the maser line shifts towards lower frequencies as t_{int} increases (see Fig. 13). This result also follows from the developed model: the red shift increases with t_{int} since a longer interaction time leads to a more adiabatic behaviour in the same way as a larger N_{ex} does.

The calculations reveal that on the vertical steps displayed in the signal the photon number distribution has two distinctly separate maxima. This situation is similar to the conditions discussed in Ref. [38], where maser field hysteresis and metastability are observed. Therefore, the maser field should exhibit hysteresis and metastability under the present conditions as well. The hysteresis should show up when the cavity frequency is linearly scanned up and down with a modest scan rate. An experimental result is shown in Fig. 15, where each step in the steady state maser line is, indeed, related to a hysteresis loop.

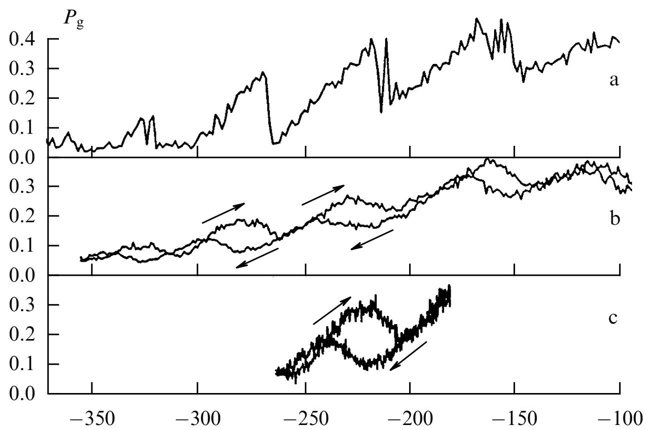

Figure 15. Hysteresis cycle of the maser. Again the atomic inversion is plotted versus the cavity frequency. (a) shows a slow scan on the red wing of the signal; (b) and (c) indicate that the vertical steps show up as hysteresis loops when the cavity frequency is rapidly scanned up and down. The scan speed: (a) 1.4 kHz, (b) 25 kHz, (c) 32 kHz; transition frequency is 21.456 GHz.

Under steady state operation of the maser on steep steps of the maser line we also observed spontaneous jumps of the maser field between metastable field states. The results displayed in Fig. 16 show that the field basically jumps between a larger and smaller field of the maser, whereby the difference in the photon numbers can be as low as 25.

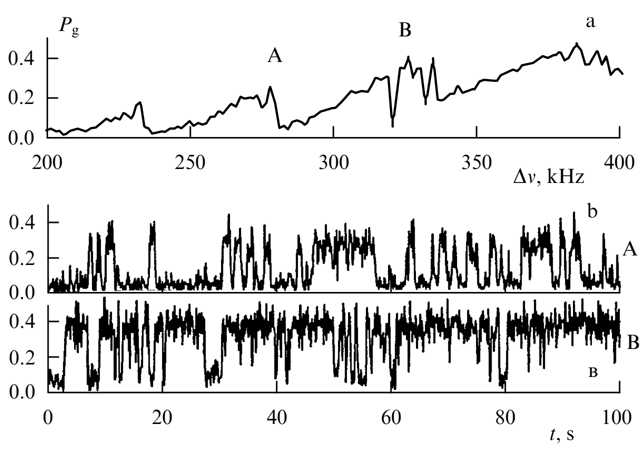

Figure 16. Spontaneous jumps of the maser field. If the maser is operated at locations A and B of the maser line (a), the atomic inversion as a function of time statistically hops (b), (c). The values Δn denote the differences of the mean photon numbers in the two metastable field states: (b) $\Delta n = 25$, (c) $\Delta n = 30$.

The calculations also show that on the smooth wings of the more pronounced interference fringes the photon number distribution $P(n)$ of the maser field is strongly sub-Poissonian. This leads to the conclusion that we are observing Ramsey-type interference induced by a nonclassical radiation field. The sub-Poissonian character of $P(n)$ results from the fact that on the smooth wings of the spikes the photon gain reduces locally when the photon number is increased. This feedback mechanism stabilises the photon number resulting in a non-Poissonian photon distribution.

In conclusion it is stated that the maser model presented explains all the observed experimental facts. The periodic structures in the maser lines are interpreted as Ramsey-type interferences. If there was more accurate information on the DC fields in the cavity, a multi-level calculation taking into account the magnetic substructure of the involved fine-structure levels would make sense. Under the present conditions, however, the stray electric field amplitudes close to the cavity holes can only be estimated. The interference structure extends towards lower frequency as far as about 500 kHz for $N_{\text{ex}} \approx 200$; this results in an electric field of about 25 mV cm^{-1} in a distance of few millimetres from the cavity holes.

In this paper we describe the first observation of Ramsey type atomic interferometry in the nonclassical field of the micromaser. To our knowledge it is the first time that it is demonstrated that non-adiabatic mixing can lead to Ramsey interferences. Besides other phenomena the bistable character of the micromaser field can be observed in jumps of the interferences; the observed interferences thus show a discontinuous behaviour owing to the quantum properties of the field — it is the first time that such a discrete quantum behaviour is directly observed in interferences. One of the applications of the described Ramsey interferometer could be the quantum non-demolition measurement of the photon number in a cavity along the lines proposed in Refs [56, 57]. For this purpose the atoms in the cavity have to be dispersively coupled to a third level via a second quantum field. The second field could be another cavity mode. Assuming that the photon lifetime of the second field is much longer than the photon lifetime corresponding to the maser transition, the number of photons in the second field can be determined from the shift of the interference patterns.

11. Linewidth and phase diffusion of the one-atom maser

In the following discussion we would like to highlight another special feature of the one-atom maser: the spectrum. It is determined by the decay of the expectation value of the electric field [41]

$$\langle E(t) \rangle \sim \sum_{n=0}^{\infty} (n+1)^{1/2} \rho_{n,n+1}(t) \,.$$

Hence the micromaser spectrum is different from the other effects discussed so far since it involves the off-diagonal elements $\rho_{n,n+1}$ of the radiation density matrix rather than, e.g., the photon statistics, i.e. the diagonal elements $\rho_{n,n}$; and it requires their time dependence rather than their steady state values. It could be shown that the linewidth D of the maser is given by

$$D = 4r \sin^2\left(\frac{g t_{\text{int}}}{4\sqrt{\langle n \rangle}}\right) + \frac{\gamma\,(2n_{\text{b}}+1)}{4\langle n \rangle} \,.$$

For small $g\tau/4\sqrt{\langle n \rangle}$ the sine function can be expanded; this leads to the familiar Schawlow–Townes linewidth

$$D = \frac{\alpha + \gamma(2n_{\text{b}}+1)}{4\langle n \rangle} \,,$$

where

$$\alpha = \gamma\big(\sqrt{N_{\text{ex}}}\, g t_{\text{int}}\big) \,.$$

The complicated pattern of the micromaser linewidth results, in part, from the complicated dependence of $\langle n \rangle$ on the pump parameter, which enters in the denominator.

We emphasise that the one-atom maser linewidth goes beyond the standard Schawlow–Townes linewidth. The sine function suggests in the limit of large pumping parameters an oscillatory behaviour of the linewidth confirmed in an exact numerical treatment. (For details see also Refs [58, 59].)

It was pointed out that the maser linewidth can be measured when two phase coupled microwave fields are used; one before the atoms enter the microwave cavity and one after, corresponding, in principle, to a modified Ramsey setup. The first micromaser field creates a superposition of the two maser states which are then probed by the second field. The first field is only applied for an initial period in order to 'seed' a phase in the micromaser cavity, while in the second field the phase diffusion is probed. This technique will provide the basis for future experiments to measure the linewidth. It was tested by computer simulations and analytical calculations which showed that coherent pumping of the maser leads to new and interesting phenomena which cannot be discussed here. The first time coherent injection for the one-atom maser was proposed in the paper by Krause et al. [60] and discussed later in connection with the measurement of the phase diffusion linewidth [61]. Also the phase dynamics of the maser field in steady state operation was discussed by Wagner et al [62]; in the latter case only one microwave field is used for probing after the micromaser cavity. The latter scheme was further pursued in connection with the entanglement of states by Wagner et al. [63]. The entangled state of the atom–field system occurs since a factorisation in field and atom part is not possible. This fact leads to applications of the micromaser for Einstein–Podolsky–Rosen type of experiments and to non-local field correlations in two distant cavities. Also the test of complementarity by means of two micromasers was discussed [64–66].

12. Microlasers

With respect to technical applications it is interesting to investigate whether similar phenomena can also be observed in cavities for optical radiation. The simplest approach to fabricating an optical microcavity is to shrink the spacing between the mirrors of a Fabry–Perot resonator to λ/n (here n stands for the refractive index) while reducing the lateral dimensions to the same range, as shown in Fig. 17. This structure provides a single dominant longitudinal field mode that radiates into a narrow range of angles around the cavity axis as indicated by the dotted line.

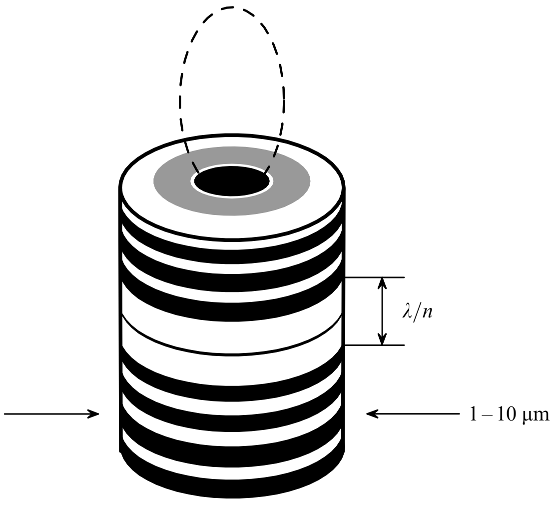

Figure 17. The Fabry – Perot microcavity being fabricated using molecular beam epitaxy to grow dielectric layered mirrors; the laser active region is the one in the middle of the region indicated at the side by λ/n (see Ref. [69]).

The first optical microcavity experiments used dye molecules between high-reflectivity dielectric mirrors in the Fabry – Perot configuration [67]. Because spontaneous emission is a major source of energy loss, speed limitations and noise in lasers, the capability to control spontaneous emission is expected to improve laser performance. If the fraction of spontaneous emission coupled into the lasing mode is made close to unit, the 'thresholdless' laser [68, 69] is obtained, i.e. the light output increases nearly linearly with the pump power instead of exhibiting a sharp turn-on at the pump threshold.

Semiconductor microcavities provide high-Q Fabry – Perot cavities for both basic studies and potential applications. Molecular beam epitaxy or organometallic chemical vapor deposition techniques are used to deposit high-reflectivity mirrors consisting of alternating quarter-wavelength layers of lattice-matched semiconductors. For example, 15 to 20 pairs of quarter-wave layers of $Al_{0,2}Ga_{0,8}As$ and AlAs result in a reflectivity greater than 99% and Q values greater than 500. The optically active layer in such a microcavity is typically a GaAs quantum well located at the midplane of the cavity, where the field strength has a maximum. Figure 17 shows an example of the very-small-diameter microcavities that can be achieved by photolithographic patterning and etching of these layered materials. For detailed review see Refs [68, 69].

Whispering gallery modes [70, 71] are a second successful route for achieving high-Q microcavities. Total internal reflection along a curved boundary between two materials with different optical indices results in high-Q modes propagating within a half-wavelength from the boundary. Semiconductor whispering gallery mode resonators have been demonstrated in disk and cylindrical geometries. For a review see Ref. [69].

It should also be mentioned here that Feld et al. recently succeeded in realising a one-atom microlaser [72]. It can be expected that this set up will also be a useful tool in testing fundamental phenomena in radiation – atom interaction.

In connection with semiconductor microcavities it is noteworthy that they have an extremely low threshold, which means that their efficiency will also be high. Low-cost, high density light source arrays and photonic circuits are possible because of the small size and low power consumption of such resonators. One will be able to produce entire wafers containing millions of microlasers with a multipole arrangement instead of having to cleave each individual semiconductor laser as at present. This improvement will lead to higher yields and lower cost per element. Another advantage of surface emitting microcavity sources is the efficient optical coupling of their stable symmetric mode patterns into optical fibres or waveguides. So it is quite certain that these lasers will cause a revolution in optical computing and in optical communication in the future.

References

1. Jaynes E T, Cummings F W *Proc. IEEE* **51** 89 (1963)
2. Haroche S, Raimond J M, in *Advances in Atomic and Molecular Physics* **20** (Eds D Bates, B Bederson) (New York: Academic Press, 1985) p. 350
3. Gallas J A C et al., in *Advances in Atomic and Molecular Physics* **20** (Eds D Bates, B Bederson) (New York: Academic Press, 1985) p. 413
4. Purcell E M *Phys. Rev.* **69** 681 (1946)
5. Drexhage K H, in *Progress in Optics* **12** (Ed. E Wolf) (Amsterdam: North-Holland, 1974)
6. De Martini F et al. *Phys. Rev. Lett.* **59** 2955 (1987)
7. Gabrielse G, Dehmelt H *Phys. Rev. Lett.* **55** 67 (1985)
8. Hulet R G, Hilfer E S, Kleppner D *Phys. Rev. Lett.* **55** 2137 (1985)
9. Jhe W et al. *Phys. Rev. Lett.* **58** 666 (1987)
10. Goy P et al. *Phys. Rev. Lett.* **50** 1903 (1983)
11. Heinzen D J, Feld M S *Phys. Rev. Lett.* **59** 2623 (1987)
12. Yamamoto Y et al., in *Coherence Amplification and Quantum Effects in Semiconductor Lasers* (Ed. Y Yamamoto) (New York: Wiley, 1991)
13. Yablonovitch E *Phys. Rev. Lett.* **58** 2059 (1987); Yablonovitch E, Gmitter T J, Bhat R *Phys. Rev. Lett.* **61** 2546 (1988); Yablonovitch E, Gmitter T J *Phys. Rev. Lett.* **63** 1950 (1989)
14. Bethe H A *Phys. Rev.* **72** 339 (1947)
15. Casimir H B G, Polder D *Phys. Rev.* **73** 360 (1948)
16. Casimir H B G *Proc. Koninkl. Ned. Akad. Wetenschap* **51** 793 (1948)
17. Hinds E A, in *Advances in Atomic, Molecular, and Optical Physics* **25** (Eds D Bates, B Bederson) (New York: Academic Press, 1990) p. 237
18. Meschede D *Phys. Rep.* **211** 201 (1992)
19. Barton G *Proc. Roy. Soc. London Ser. A* **410** 141, 175 (1987)
20. Sukenik C I et al. *Phys. Rev. Lett.* **70** 560 (1993)
21. Wegener T, Dirscherl J, Walther H *Opt. Commun.* **91** 131 (1992)
22. Wegener T *Thesis* (Munich: University of Munich, 1994)
23. Dobiasch P, Walther H *Ann. Phys.* (France) **10** 825 (1985)
24. Heinzen D J et al. *Phys. Rev. Lett.* **58** 1320 (1987)
25. Meschede D, Walther H, Müller G *Phys. Rev. Lett.* **54** 551 (1985)
26. *See, for example,* Eberly J H, Narozhny N B, Sanchez-Mondragon J J *Phys. Rev. Lett.* **44** 1323 (1980), *and references therein*
27. Rempe G, Walther H, Klein N *Phys. Rev. Lett.* **58** 353 (1987)
28. Meystre P, in *Progress in Optics* **30** (Ed. E Wolf) (Amsterdam: North-Holland, 1992) p. 261
29. Filipowicz P, Javanainen J, Meystre P *Opt. Commun.* **58** 327 (1986); *Phys. Rev. A* **34** 3077 (1986); *J. Opt. Soc. Am. B* **3** 906 (1986)
30. Lugiato L A, Scully M O, Walther H *Phys. Rev. A* **36** 740 (1987)
31. Meystre P *Opt. Lett.* **12** 669 (1987); Meystre P, in *Squeezed and Nonclassical Light* (Eds P Tombesi, E R Pike) (New York: Plenum, 1988) p. 115
32. Meystre P, Wright E M *Phys. Rev. A* **37** 2524 (1988)
33. Rempe G, Walther H *Phys. Rev. A* **42** 1650 (1990)
34. Paul H, Richter Th *Opt. Commun.* **85** 508 (1991)
35. Rempe G, Schmidt-Kaler F, Walther H *Phys. Rev. Lett.* **64** 2783 (1990)
36. Briegel H J et al. *Phys. Rev. A* **49** 2962 (1994)
37. Wagner C, Schenzle A, Walther H *Opt. Commun.* **107** 318 (1994)
38. Benson O, Raithel G, Walther H *Phys. Rev. Lett.* **72** 3506 (1994)
39. Davidovich L et al. *Phys. Rev. A* **36** 3771 (1987); Brune M et al. *Phys. Rev. Lett.* **59** 1899 (1987)

40. Meystre P, Rempe G, Walther H *Opt. Lett.* **13** 1078 (1988)
41. Raithel G et al., in *Advances in Atomic, Molecular, and Optical Physics* Suppl. 2 (Ed. P Berman) (New York: Academic Press, 1994) p. 57
42. Yoo H I, Eberly J H *Phys. Rep.* **118** 239 (1985)
43. Knight P L, Radmore P M *Phys. Lett. A* **90** 342 (1982)
44. Kimble H J, Walls D F *J. Opt. Soc. Am. B* **4** 1449 (1987)
45. Loudon R, Knight P L *J. Mod. Opt.* **34** 709 (1987)
46. Kimble H J, Dagenais M, Mandel L *Phys. Rev. Lett.* **39** 691 (1977); *Phys. Rev. A* **18** 201 (1978)
47. Cresser J D et al., in *Dissipative Systems in Quantum Optics* (Berlin: Springer, 1982) p. 21
48. Short R, Mandel L *Phys. Rev. Lett.* **51** 384 (1983)
49. Diedrich F, Walther H *Phys. Rev. Lett.* **58** 203 (1987)
50. Slosser J J, Meystre P, Wright E M *Opt. Lett.* **15** 233 (1990)
51. Carmichael H J, Walls D F *J. Phys. B* **9** (8) 1199 (4) L43 (1976)
52. Krause J, Scully M O, Walther H *Phys. Rev. A* **36** 4547 (1987); Krause J, Scully M O, Walther T, Walther H *Phys. Rev. A* **39** 1915 (1989)
53. Braginsky V B, Khalili F Y, in *Quantum Measurement* (Cambridge: Cambridge Univ. Press, 1992)
54. Ramsey N F, in *Molecular Beams* (Oxford: Clarendon Press, 1956)
55. Cohen-Tannoudji C, Dupond-Roc J, Grynberg G, in *Atom – Photon Interactions* (New York: John Wiley and Sons Inc., 1992)
56. Brune M et al. *Phys. Rev. Lett.* **65** 976 (1990)
57. Haroche S, in *Fundamental Systems in Quantum Optics* (Eds J Dalibard, J M Raimond, J Zinn-Justin) (Amsterdam: Elsevier, 1991)
58. Scully M O et al. *Phys. Rev. A* **44** 5992 (1991)
59. Quang T et al. *Phys. Rev. A* **48** 803 (1993); Vogel K et al. *Phys. Rev. A* **48** 813 (1993)
60. Krause J, Scully M O, Walther H *Phys. Rev. A* **34** 2032 (1986)
61. Brecha R J et al. *Phys. Rev. A* **46** 567 (1992)
62. Wagner C et al. *Phys. Rev. A* **46** R5350 (1992)
63. Wagner C et al. *Phys. Rev. A* **47** 5068 (1993)
64. Scully M O, Walther H *Phys. Rev. A* **39** 5229 (1989)
65. Scully M O, Englert B-G, Walther H *Nature* (London) **351** 111 (1991)
66. Englert B-G, Walther H, Scully M O *Appl. Phys. B* **54** 366 (1992)
67. De Martini F, Jacobovitz G R *Phys. Rev. Lett.* **60** 1711 (1988)
68. Yokoyama H *Science* **256** 66 (1992)
69. Yamamoto Y, Slusher R S *Physics Today* **46** 66 (1993)
70. Braginsky V B, Khalili F Y *Phys. Lett. A* **186** 15 (1994)
71. Braginsky V B, Gorodetsky M L, Khalili F Y *Phys. Rev. Lett. A* **191** 208 (1994)
72. An K et al. *Phys. Rev. Lett.* **73** 3375 (1994)